



Research paper

Applying Partial Differential Equations on Cubic Uniform Local Binary Pattern to Reveal Micro-Changes

V. Esmaili¹, M. Mohassel Fegghi^{1,*}, S. O. Shahdi²

¹ Faculty of Electrical and Computer Engineering, University of Tabriz, Tabriz, Iran.

² Department of Electrical Engineering, Qazvin Branch, Islamic Azad University, Qazvin, Iran.

Article Info

Article History:

Received 23 August 2023
Reviewed 12 October 2023
Revised 07 November 2023
Accepted 04 December 2023

Keywords:

Apex
Cubic-ULBP
Micro-Changes
Micro-Expression
Partial Differential Equations (PDE)

*Corresponding Author's Email Address:
mohasselfegghi@tabrizu.ac.ir

Abstract

Background and Objectives: The world we live in everyday, accompany with enormous numbers of minute variations which affect us and our surroundings in several aspects. These variations, so called micro-changes, are low in intensity and brief in duration which makes them almost invisible to naked eyes. Nonetheless, revealing them could open up a new wide range of applications from security, business, engineering, medical, and seismology to psychology.

Methods: In this paper, we adopted a novel autonomous approach comprising Partial Differential Equations (PDE) and Cubic Uniform Local Binary Pattern (Cubic-ULBP) to spot micro-changes. Cubic-ULBP extracts 15 planes containing robust features against noise and illumination variations. Afterwards, PDE pick out single plane out of 15 to reduce time consumption.

Results: The proposed method is not only optimized to get the job done perfectly but also provides promising results comparing with most state-of-the-art methods. So that the accuracy is increased about 36% and 40% on the CASME and the CASME II databases, respectively.

Conclusion: The combination of the PDE and the Cubic-ULBP creates a strong and optimal method for detecting the apex frame and micro-movement. This method's performance is found to be promising when the training samples are scarce, too.

This work is distributed under the CC BY license (<http://creativecommons.org/licenses/by/4.0/>)



Introduction

The micro-changes take place frequently in various environments, which their existence could be confirmed through elaborate analysis of the video frames. Meanwhile, the human eyes cannot see such trifle changes since they appear in fraction of second/s without clear perceptible features. Undoubtedly, spotting them is advantageous to many applications such as security, engineering, medical, judicial, nanotechnology seismology, psychology, and etc.

Ekman and Friesen are believed to be the first

researchers who unveil facial micro-changes when they were scrutinizing video frames in 1969 [1]. These micro-changes appear on face both instantaneous and spontaneous against person willingness to suppress them. Besides, their characteristics make micro-changes, known as micro expression, genuine and real [2]-[3]. Hence, such nonverbal leakage could be regarded as a strong clue for the act of lying and deception [1], [4]-[8].

Although spotting such a low intensity and moment facial muscle deformity is not an easy task, revealing them paves the long way for court authorities to discern honest

from lying culprits and/or witnesses. Moreover, with these micro-expression symptoms, psychologists can early diagnose patients with depression and other mental health difficulties. As a result, it could play a vital role to avoid suicide or related mental disease aftermath. In the same manner, within educational systems, teachers could measure their training efficacy with extracting student micro-expressions.

The micro-changes are not limited to micro expression, but to other key areas. In another case, we could locate micro-change features when smoke is arisen above the mouth of a volcano. The amount of smoke can determine the rate of volcano activity [9], [10]. Surprisingly, one could even foresee the earthquake by timely detecting subtle and micro smoke changes [11], [12]. Therefore, casualties caused by great destruction due to volcanic actions are diminished significantly, and human lives are saved.

In more direct connection with human health, spotting micro-changes in blood circulation can aid diagnosing some of the most prevalent medical diseases. As an example, a cardiac arrhythmia is high probable when person has an irregular heartbeat, i.e. too slow, or too fast [13], which could be stemmed from heart disease [14]. Also, monitoring heartbeat or pulse can determine palpitations and locate local blood vessels. In fact, their visibility comes from micro-changes of blood which flows in arteries closed to the surface of skin.

In retrospect, detection of such micro-changes could result in making concise decision for wide range of applications. Nevertheless, this task is an arduous and requires professional expertise or autonomous setup. One could spot micro-changes with high attention over time well. For further clarification, assume a phenomenon including micro-changes. When each image has taken into probe individually, they look all the same. However, when we compare them together over time, their minute disparities would be discovered.

This minute scale changes, which are occurred in various locations and multi-orientations within image frames, impose severe detection challenge. Their subtle changes are indiscernible from shadows, noises, and other similar features. As a result, the performance of spotting micro-changes is subsided significantly with the presence of noise or equally by low-rate of the signal to noise ratio (S/N).

It is noteworthy to mention that among the sequence of frames; one single frame has the highest fluctuations in features with respect to others. This frame is known as the peak or apex, which is very crucial to locate. It can convey the strongest signal and main message. For instance, a single apex represents vital information with the video capture of micro-expressions at 200 fps. It contains sufficient meaningful information which could

be then interpreted as a specific micro-expression [15], [16]. The rest of the frames demonstrate nearly a neutral expression of the face, or less deviated from neutral compare to apex. Hence, analyzing all of the frames rather than just apex increases the burden of processing without a fruitful outcome.

The apex frame, also in the case of volcano, contains the maximum smoke coming out of a crater which could be used to approximate the time of probable earthquakes. In another case, the apex frame makes it easy to locate blood vessels under the skin. This process alleviates injecting donated blood, blood products, or other necessary fluids into the circulatory system.

Since the direction of micro-change is unpredictable, all possible orientations must be considered. Thus, promising textural algorithms, like Local Binary Pattern on Three Orthogonal Planes (LBP-TOP) [17], are not satisfying for the micro-changes analysis. They are imperfect since they merely take data in two directions (i.e. vertical and horizontal) over time.

Instead of three planes in the limited directions, the Cubic-LBP [4] comprising 15 planes in multiple directions which potentially grasp any changes in multi-directions. Nevertheless, both the LBP-TOP and the Cubic-LBP adversely affected by illumination variations and noises as they exert the simple LBP [18] on their planes. Using Uniform LBP (ULBP) [19] rather than the simple one can discard the interference of illumination variations and shadows in micro-change spotting process. Also, processing 15 planes in Cubic-LBP has more computation. Therefore, it is very time-consuming.

In 2020, Esmaili and shahdi [4] tried to find the apex frame containing the micro-changes in the CASME II and the CASME. In their work, the error was about 6.5 frames from the truth apex in the CASME II. Furthermore, there was around two frames error in the CASME. Then, in [6], the use of the diagonal planes not only reduced the error but also led to simple calculations. However, there were still six frames far away from the ground truth in the CASME II. In the next work [20], a method called the LBP on six intersection planes had only 1.7 errors in the CASME.

In 2022, a method based on the deep learning named as the intelligent cubic-LBP [21] has been presented for spotting the micro-changes on the datasets such as the FA and the POVI. Nevertheless, the convolutional neural networks often require complex computation and the high processing/learning time [22]-[26].

In this paper, we present a novel approach to detect the micro-changes. Our goal is to bring the Cubic-ULBP and the Partial Differential Equations (PDE) together for the sake of reaching outstanding outcomes. In fact, the major contribution of this paper is to extract robust features against noises through the Cubic-ULBP.

Furthermore, the proposed method automatically selects only one plane out of the 15 Cubic-LBP planes using the PDE, to reduce the processing time. This single plane highlights the main direction of the micro-changes. Our extensive experiments on datasets prove the competitiveness of the proposed method, which is optimized to contests with the related state-of-the-arts.

Related Works

A plethora of phenomena is tending to cause changes, movements, and motions that are still subtle in nature [27]. Even though, they are too small to distinguish by the human visual system accurately. In order to address this limitation, researchers have suggested various methods to tackle this problem which ends up with detecting minute spatial and temporal variations [4], [28]-[30].

The Lagrangian method is considered to be one of them. It tracks movement or motion in a video frames [28], [31]. The principle of this method is based on magnifying movements of fine point which consequently become more visible to the naked eye. However, poor estimated movements and sensitivity to spatial noise are among its drawbacks.

The other motion magnification method is called Eulerian that is used in multiple fields [29], [32]-[34]. Beside magnification, it also reveals micro-color changes [28]. Deteriorating by captured noise, computationally-intensive, and unsuitability for high-frequency bands are its general disadvantages. Unlike Lagrangian, the Eulerian doesn't support large amplification factors.

On the contrary, phase-based video motion processing approach [27] is robust against noise due to phase magnification rather than feature magnification. However, because of its complexity, the huge processing burden is imposed on such system.

The other intricate method is the complex wavelet (CWT), which is optimized to magnify micro-movement [29]. Under this approach, any micro-change in any direction over time is magnified by the CWT decomposition band.

Two later methods mentioned above rely on the frequency decomposition.

To resolve the complexity problem, LBP-based methods such as Cubic-LBP [4] have been introduced. Nonetheless, they have deficiencies that should be get rid of them.

These are sensitive to the illumination variations, the shadow variations, and the noises. It is in order to come up with aforementioned shortcomings, we adopt an optimized approach comprising Cubic-ULBP and PDE.

The Cubic-ULBP is not only simple in computation but also can track any given direction of the micro-change. On top of that, it is insensitive to noise and illumination variations.

Unfortunately, the Cubic-ULBP has relatively high

number of planes, i.e. 15 planes. To eliminate this problem, the PDE is then called to choose just single plane. Therefore, volume of computation becomes even simpler. It is worthwhile to bear in mind that PDE has other applications in image processing such as denoising, image enhancement, and tracking as reported in [35]-[40].

Proposed Method

We extract features from the consecutive images using a texture-based method, namely Cubic-ULBP. Then, the maximum direction of micro-changes would be determined.

More specifically, the PDE selects a single plane among 15 that reveals the most micro-changes. Finally, the apex frame is spotted by evaluating the discrepancy between the histogram of each frame and the normal frame in that single plane.

The general framework of our proposed method is shown in Fig. 1.

A. Cubic-ULBP

We use frames as image sequences. These standard images are put successively such that construct a three-dimensional array. 15 planes encompass the pixels in multi-directions. They are named Cubic method planes as depicted in Fig. 2.

There are 3 separate planes in directions of XT, XY, and YT.

Also, there are 6 diagonal planes in the cuboid. Except for the XY orientation planes, the rest of them collect pixels from consecutive images. It is prerequisite to convert the color images to the grayscale for ULBP process.

Suppose pixels (P_s , for $s=1$ to NuP) are located on a circle with R radius in a plane. The number of P_s (NuP) is selected to attain the best performance.

If we consider that the middle point of the circle to be a pixel C , then, the location of each P_s on every plane is defined as follow:

$$(x_c + Ra_x \cos(I), y_c - Ra_y \sin(I), t_c) \tag{1}$$

$$(x_c + Ra_x \cos(I), y_c - Ra_y \sin(I), t_c \pm S) \tag{2}$$

$$(x_c, y_c - Ra_y \sin(I), t_c + Ra_t \cos(I)) \tag{3}$$

$$(x_c \pm Ra_x, y_c - Ra_y \sin(I), t_c + Ra_t \cos(I)) \tag{4}$$

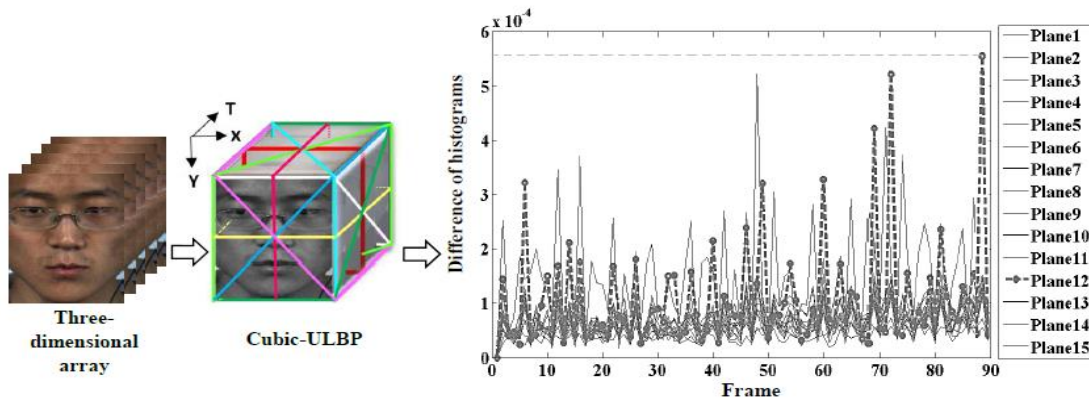
$$(x_c + Ra_x \cos(I), y_c, t_c + Ra_t \sin(I)) \tag{5}$$

$$(x_c + Ra_x \cos(I), y_c \pm Ra_y, t_c + Ra_t \sin(I)) \tag{6}$$

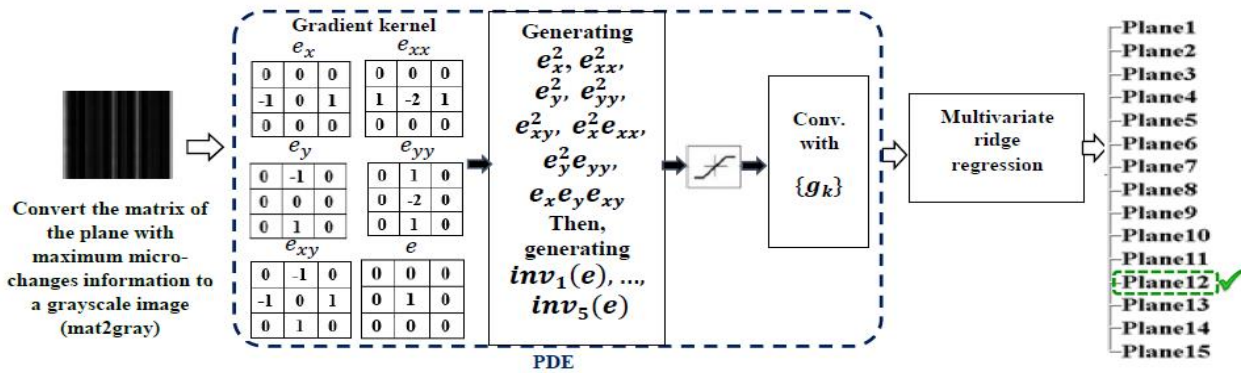
$$(x_c + Ra_x \sin(I), y_c - Ra_y \sin(I), t_c - Ra_t \cos(I)) \tag{7}$$

$$(x_c - Ra_x \sin(I), y_c - Ra_y \sin(I), t_c + Ra_t \cos(I)) \tag{8}$$

Stride 1. Specifying a plane with maximum micro-changes information among 15 planes of Cubic-ULBP



Stride 2. Learning PDE and classification for selecting a single plane



Stride 3. Spotting the apex (a frame that shows the maximum micro-changes) by only the selected plane

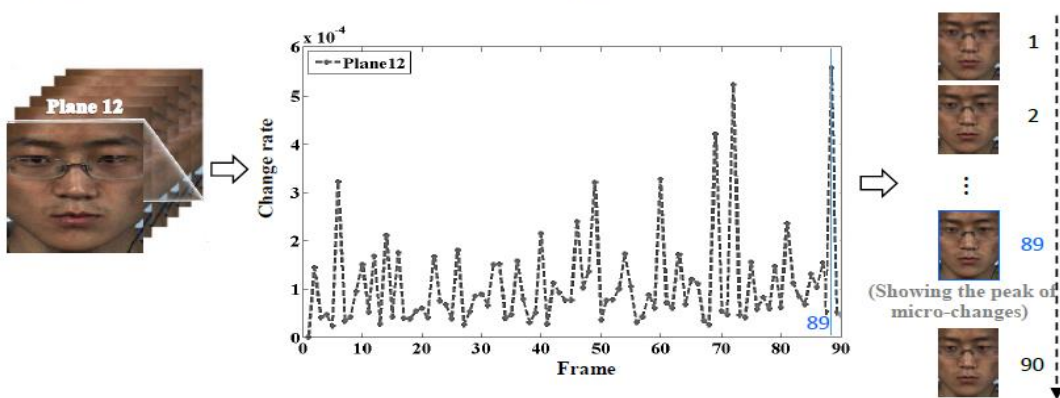


Fig. 1: The general framework of our proposed method.

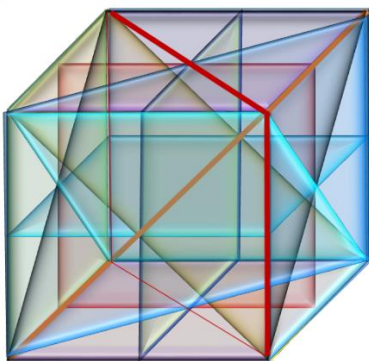


Fig. 2: Cubic method planes.

$$(x_c + Ra_x \cos(I), y_c - Ra_y \sin(I), t_c + Ra_t \sin(I)) \quad (9)$$

$$(x_c - Ra_x \cos(I), y_c - Ra_y \sin(I), t_c - Ra_t \sin(I)) \quad (10)$$

$$(x_c + Ra_x \cos(I), y_c - Ra_y \sin(I), t_c - Ra_t \cos(I)) \quad (11)$$

$$(x_c + Ra_x \cos(I), y_c - Ra_y \sin(I), t_c + Ra_t \cos(I)) \quad (12)$$

where I equal to $2\pi P/NuP$ and S is the interval on T axis.

In the ULBP routine, P_s values are subtracted by the value of C . Then, the positivity of outcome is checked. If it holds true, it would be exchanged by "1" and otherwise

replaced by "0". Thereafter, these binary values concatenated together to create specific pattern (e.g. 01101001).

In order to discern uniform from non-uniform patterns, we build a histogram of ULBP. For this purpose, number of reciprocal transitions between 0 and 1 are enumerated. If there are just 2 or less transitions, the pattern is put into uniform bin. A separate bin is assigned for all non-uniform patterns which have more than two transitions. This task provides the feature vector, well known as histogram of ULBP.

In comparison with ordinary LBP [18], ULBP ends up in shorter feature vector. It could be obtained through following equation:

$$e_q(x,y,t) = 0, \quad (x,y,t) \in \partial\Psi \times [0,Ti]$$

$$Uniform\ LBP = |sign(Val_{NuP} - Val_C) - sign(Val_0 - Val_C)| + \sum_{P=1}^{NuP-1} |sign(Val_P - Val_C) - sign(Val_{P-1} - Val_C)| \quad (13)$$

$$HistULBP = \begin{cases} \sum_{P=0}^{NuP-1} sign(Val_P - Val_C) & \text{if } Uniform\ LBP_{NuP,Ra} \leq 2 \\ NuP + 1 & \text{otherwise} \end{cases} \quad (14)$$

To get a coherent description, the normalized histogram of the Cubic-ULBP is computed by concatenation of ULBP features on the planes as follow:

$$NormHist_{\varphi,h} = \frac{\sum_{x,y,t} J\{Uniform\ LBP_{\varphi}(x,y,t) = \varphi\}}{\sum_{\omega=0}^{q-1} HistULBP_{\omega,h}} \quad (15)$$

where φ is a factor which is confined between 0 and the number of ULBP labels in the plane (q). The h is plane number (i.e. $h: 1, 2, \dots, 15$). $J(\cdot)$ is 1 when (\cdot) is true, and it is 0 otherwise.

The Cubic-ULBP histogram is comprised of 15 histograms; each one belongs to specific counterpart plane. In most cases, only one plane out of 15 planes carries information with the most micro-changes. It can be explained mathematically as:

$$\sum_1^{NF} (NormHist_{fi} - NormHist_f)^2 \quad (16)$$

where fi , NF , and f are the frame of interest, number of frames, and frame1 respectively. With frame1, we mean a normal frame, containing no change, which is often happened to be the first frame [41], [42].

B. PDE

Histogram of a plane with the most micro-changes is captured as a matrix (\mathbf{v}). The histogram, which is obtained from Cubic-ULBP in previous section, is processed again

to create vector \mathbf{v} . Thereupon, the \mathbf{v} is inserted into the PDE and its features are extracted as output (o). The PDE is defined as:

$$\frac{\partial e_q}{\partial t} = L(e,x,y,t), \quad (x,y,t) \in \Psi \times [0,Ti]$$

$$e_q|_{t=0}(x,y,t) = \mathbf{v}_q, \quad (x,y) \in \Psi \quad (17)$$

where $q=1, 2, \dots, Q$. The Q is the number of samples and Ψ is the rectangular region in R^2 . The e and Ti are the evolution of the \mathbf{v} and feature extraction process time by the PDE respectively. The feature map $e / t = T$ has a similar dimension as the \mathbf{v} . If the gradient and hessian of the \mathbf{v} are $\nabla \mathbf{v}$ and \mathbf{H}_v , then the PDE can be formulated as:

$$\frac{\partial e}{\partial t} = L(e,\nabla \mathbf{v},\mathbf{H}_v) \quad (18)$$

We deduce the L feature inspired by [40]. The PDE shares the same characteristics with Cubic-ULBP which both are illumination and rotation invariant. In fact, we use the rotational invariants up to the second order. The input and desired output are as follows, respectively:

$$inv_0(e) = 1 \quad (19)$$

$$inv_1(e) = e \quad (20)$$

The squared norm of the gradient is as:

$$inv_2(e) = \|\nabla e\|^2 = e_x^2 + e_y^2 \quad (21)$$

Also, the Laplacian is as follows:

$$inv_3(e) = tr(\mathbf{H}_e) = e_{xx} + e_{yy} \quad (22)$$

A visual front-end operation is as:

$$inv_4(e) = (\nabla e)^{Ti} \mathbf{H}_e \nabla e = e_x^2 e_{xx} + 2e_x e_y e_{xy} + e_y^2 e_{yy} \quad (23)$$

In addition, a deviation from flatness is as following:

$$inv_5(e) = tr(\mathbf{H}_e^2) = e_{xx}^2 + 2e_{xy}^2 + e_{yy}^2 \quad (24)$$

To get approximate invariant under gray-level scaling, the term $a(x) = \frac{x}{1+|x|}$ is added to each differential invariant. Thus, the differential invariants becomes as $\{a(inv_{0\ to\ 5}(e))\}$. Consequently, L can be written as a function of them:

$$L(e,t) = \sum_{k=0}^5 g_k(t) a(inv_k(e(t))) \quad (25)$$

$g_k(t)$ is independent of the (x, y) in (25). It is to minimize the loss function.

C. Classification

Now, a simple linear classifier is required for the classification purpose which is fed by PDE outcomes. We use the multivariate ridge regression [39], [40] in order to reduce complexity.

In the training step, we minimize a loss function to get optimized values for the parameters (W) and L . Training samples are the input matrixes (\mathbf{v}_q) and their

corresponding tag vector (d_q) that belongs to class h . For each input, we compute a feature map using (17). If the regularization term set to be G , then the whole learning features can be extracted as follow:

$$\min_{\{g_{k(t)}\}, \mathbf{W}} E = \frac{1}{Q} \sum_{q=1}^Q \text{LOSS}(\mathbf{W}; e_{q|t=Ti}, d_q) + \lambda G(\mathbf{W}) \quad (26)$$

where lambda (λ) is a trade-off parameter. The extracted features are chosen in order to minimize the loss function. More clearly, the PDE learns the $\{g_{k(t)}\}$ and W parameters. The aim in (26) is to learn the multivariate ridge regression as:

$$\min_{\mathbf{W}, L} E = \frac{1}{Q} \|D - \mathbf{W} \cdot \mathbf{V}|_{t=Ti}\|_L^2 + \lambda \|\mathbf{W}\|_L^2 \quad (27)$$

where $D = [d_1, d_2, \dots, d_Q]$, and $\mathbf{V}|_{t=Ti} = [\text{vect}(e_1|_{t=Ti}), \dots, \text{vect}(e_Q|_{t=Ti})]$. For the multivariate ridge regression, the size of the W matrix is the number of categories multiplied by the number of the input image pixels. The class label for each test image can be achieved as follows:

$$\text{label} = \arg \max\{\mathbf{W} \cdot \text{vect}(e|_{t=Ti})\} \quad (28)$$

To solve (27), $\{\mathbf{v}_q, d_q\}_{q=1}^Q$, λ , and the step size during optimization (μ) are selected as inputs. To achieve best overall results, $\Delta t, N, \beta, \varepsilon, \gamma$, and γ_{max} are initialized to 0.5, 5, 0.95, 10-6, 1, and 10, respectively. Besides, Λ is initialized with each entry uniformly sampled from $[-1, 1]$. To accomplish classification task, we perform five steps while $\gamma \leq \gamma_{max}$ and $\|E^\gamma - E^{\gamma-1}\| > \varepsilon$:

- 1) Set $e_q^0 = \mathbf{v}_q$ and calculate $e_q^{\zeta+1} = e_q^\zeta + \Delta t \sum_{k=0}^5 g_k^\zeta \cdot a(\text{inv}_k(e_q^\zeta))$, $\zeta = 0, 1, \dots, N - 1$;
- 2) Solve $\mathbf{W} = \arg \min_{\mathbf{W}} \frac{1}{Q} \|D - \mathbf{W} \cdot \mathbf{V}^N\|^2 + \lambda \|\mathbf{W}\|_L^2 = D \cdot (\mathbf{V}^N)^{Ti} \cdot [\mathbf{V}^N \cdot (\mathbf{V}^N)^{Ti} + \lambda Q \eta]^{-1}$;
 $\eta \in \mathbb{R}^{\text{the pixel number of an image} \times \text{the pixel number of an image}}$
- 3) Update Λ by one gradient descent as $(g_k^\zeta)^{\gamma+1} = (g_k^\zeta)^\gamma - \mu \frac{\partial E^\gamma}{\partial (g_k^\zeta)^\gamma}$;
- 4) Update $\mu = \beta \mu$;
- 5) Update $\gamma = \gamma + 1$.

Experimental Results

All experiments are implemented in MATLAB 2020b under Windows 7 on a PC equipped with a 3.5GHz CPU and 8GB RAM. We begin this section with describing the datasets which are used in our research. Thereafter, the settings and also implementation details are provided to accommodate the necessity of procedure replication. In last, we present an extensive investigation on results which then being compared to the most state-of-the-art

methods.

A. Datasets Specifications

The Chinese Academy of Sciences Micro-Expressions (CASME) [41] and its extended version, namely CASME II [42] are among most widely used datasets. One of particular reason behind this popularity is the liable labels including apex frame. Specially, these pre-labelled apex frames lead to a concise evaluation of our proposed method. The earlier dataset has more than 190 samples each one contains of dozens consecutive facial images. The latter, which is bigger in size, has more than 240 samples.

As it is appeared in Fig. 3, the apex frame demonstrates relatively high degree of variations in comparison with the other frames. More specifically, in this figure, the emotion of disgust is most discernable within forehead area in the apex frame.

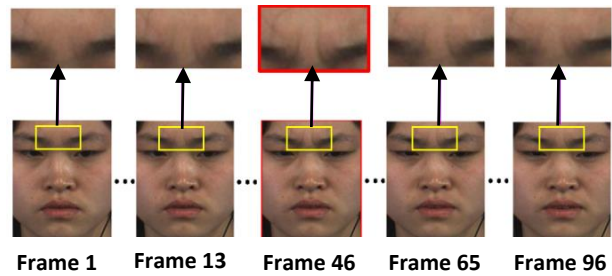


Fig. 3: A sample of disgust expression from the CASME II dataset. In this sample, the forty-sixth frame shows the most muscle contraction within the forehead area in comparison to others. Thus, it is the exact apex with the most micro-changes information.

Although the resolution of these datasets (1280×720 for CASME and 280×240 for CASME II) satisfies our system requirements, there are still some other motions which should not be regarded as micro-changes. In order to overcome these defects, we manually omit the samples with the motions that are not mainly categorized as micro-changes. The third dataset which we manage to exploit in our proposed method is named POVI¹ [43]. It is video data which captured the activity of Villarrica volcano. A sample of image sequence from this dataset is illustrated in Fig. 4. It should be mentioned out that just the portion of this dataset which is in accordance with micro-changes of volcano activity is utilized.

We take advantage of the last dataset that is corresponding to retinal blood vessels. They were collected from the retinal Fluorescein Angiography (FA) [44]. For each instance in this dataset, there are at least 110 frames available. The main drawback with this dataset is the lack of apex frame labels which leaves researchers with no choice rather than tagging them manually.

¹ <http://www.povi.cl/>

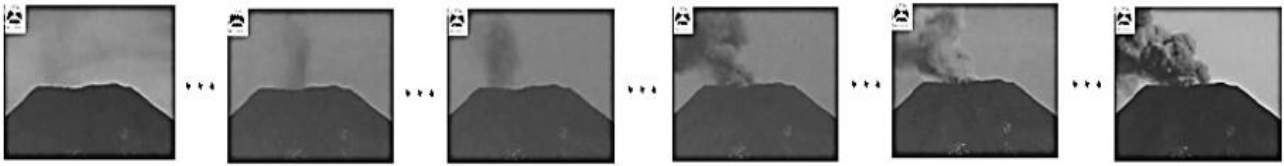


Fig. 4: A sample of consecutive images from the POVI.

B. Simulation Details

Initially, image frames of one sample are clustered with the length of three frames. This task proceeds by separating triple frames starting from onset frame into the offset one. To be sure not to miss any micro-change, this process is accomplished through an overlapping scheme where a frame could be considered multiple times. Thus, the interval on the T axis (S) is set to be 1. Besides, for the textural analyzer like ULBP to be applicable, all images should be first transformed into the grayscale level. As discussed in section III-A, cubes are made from clusters of 3 consecutive frames. Afterwards, 15 planes are extracted from each Cube to encompass every possible motion in multi-directions. It could be perceived from Fig. 5 that eight pixels including $P1, P2, \dots,$ and $P8$ are located on a circumference of a circle with a $Ra=1$ radius. It means that the NuP is eight. The Ra and NuP have been selected according to the best performance. In order to apply ULBP, each pixel on the circle circumference is subtracted from the center C value. With this subtraction results, the string of binary codes is then created where positive and negative values of subtractions are exchanged with 1 and 0 respectively. If there are only 2 or less transition existed between zeros and ones within code string, this pattern is classified as uniform. Consequently, a separate bin is assigned for these uniform patterns in the ULBP histogram. The rest of the patterns, namely non-uniform patterns, are located into another single bin.

At last, all the histograms, which are extracted from 15 distinct planes, are concatenated to make the single Cubic-ULBP histogram. This histogram is then placed into a matrix of 15 rows in which each row stands for a specific plane. In other words, the ULBP histograms of plane 1 up to plane 15 are in turn the first row up to the last row of the matrix. Therefore, this matrix contains the entire textural features extracted from a sample video data by the means of Cubic-ULBP.

Now, we probe variations by looking into histogram matrix using (16). Thus, the plane with the maximum micro-changes is spotted when its variation is compared with the rest of the frames. This plane could pave the significant way to locate micro-changes since it has relatively high amount of valuable data. For example, plane number 13 in Fig. 5 has the same characteristic and outweigh in variations over other planes.

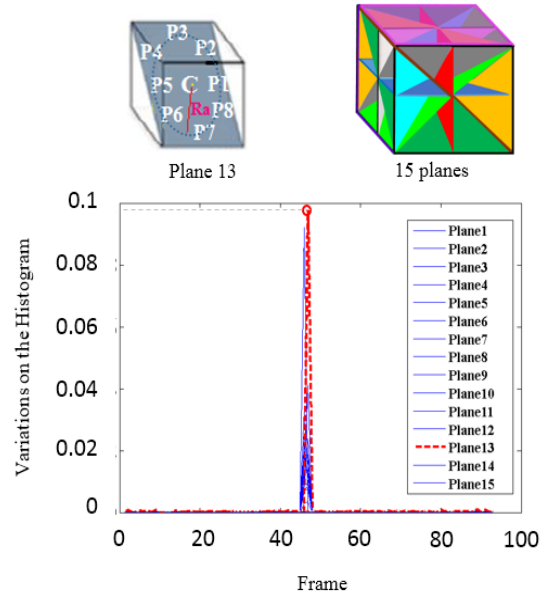


Fig. 5: The histograms variation using 15 planes in consecutive images.

In the next step, this plane's information is fed into the PDE, and in this example its corresponding tag is set to be 13. This procedure is iterated similarly for all other samples through the dataset.

The PDE parameters are trained to learn from features of the matrix according to part B of section III. We minimize the loss function for determining the parameters. The multivariate ridge regression is then utilized as a classifier. Training sets include histogram matrix as an input and its corresponding tag vector, which belongs to class h , as an output. As a result, there are 15 classes where the $h1$ as class 1 belongs to plane 1 and $h15$ as class 15 belongs to plane 15. Fortunately, the direction of micro-changes is also unraveled by this class.

For each plane, we randomly select 15 matrixes for training and the rest are selected for testing. In our method, the hyper-parameters of λ (i.e., regularization parameter) and μ (i.e., step size during optimization) are tuned to obtain the best performance. Since in most cases the training samples are limited, λ and μ are chosen from $\{1, 1.5, 5, 10, 50\}$ and $\{0.1, 0.3, 0.5, 0.7, 0.9\}$, respectively [32]. We choose λ of 1.5 and μ of 0.5 for this purpose. We set them due to the best achieved spotting accuracy. Fig. 6 shows two samples of the effects of selecting λ and μ value on apex spotting accuracy on the used data.

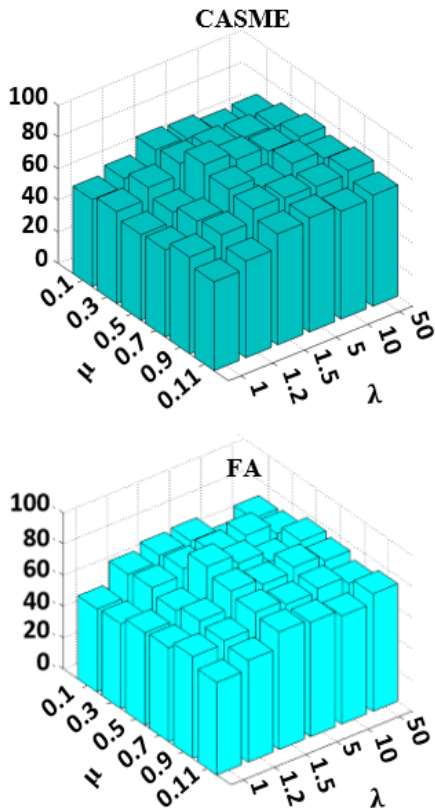


Fig. 6: The effects of λ and μ on apex spotting accuracy.

Therefore, the PDE pick out a single plane out of 15 that reveals the most micro-changes. Finally, the apex frame is spotted by evaluating the discrepancy between the histogram of each frame and the first frame (i.e., normal frame) in that single plane.

C. Discussion on Experimental Results

According to our results, the proposed method outperforms over other state-of-the-art researches in spotting the apex frame. Even more, its performance is found to be promising when the training samples are scarce. Meanwhile, the large amounts of training samples are often required for the well-known methods (such as the method presented in [21], [23], [26]). Collecting such enormous samples is not always easy and cost effective. Our proposed method not only overcomes this challenge, but also reaches better efficiency compared to the other approaches.

Besides, in terms of optimization, our proposed method has a clear advantage over customary Cubic-LBP since it selects merely a single plane rather than 15. In consequence, the computation process of our method is slashed significantly.

Unsurprisingly, with the characteristics of ULBP and PDE, our method is more robust against illumination variations. This robustness is mainly due to three reasons. First, we use a uniform pattern in ULBP that relatively discards effect of illumination variations. Second, the PDE parameters are learned with the features extracted from

an illumination invariant histogram. Third, we add the term $a(x)$ on each differential invariant which ends up with more insensitivity to the illumination fluctuations.

Table 1 reports the apex spotting accuracy in percentage on the CASME dataset with 15 training samples. We can see that the apex frame spotting accuracy is increased by more than 35% in the experiments on the CASME in comparison with [2], [3], and [16], [17]. In order to further validate our method, the experiments are repeated on the CASME II.

Table 2 demonstrates micro-changes spotting accuracy on this dataset with just 15 training samples. Again, as it could be perceived from this table, the accuracy which is achieved by our method, in comparison with others, is improved noticeably.

In addition, we also conduct the experiments to come up with apex spotting in the POVI and FA. Their results are summarized in Table 3. Furthermore, the assessment of wrong apex spotting is computed through the mean absolute error as follow:

$$\text{mean absolute error} = \frac{1}{Q} \sum_1^Q |\text{deviation}| \quad (29)$$

Besides, we achieve the standard error as follow:

$$\text{standard error} = \frac{\text{sample deviation}}{\sqrt{Q}} \quad (30)$$

Results on both mean absolute error and standard error which are given in Table 4 are comparatively negligible. In Fig. 7 we picture a clear view of the superiority of our proposed method comparing with other related methods. Moreover, the proposed method (combining PDE and Cubic-ULBP) efficiency is measured using precision (prec.), recall (rec.), and F1 metrics [45] as follows:

$$\text{rec.} = \frac{\text{TruePos.}}{\text{FalseNeg.} + \text{TruePos.}} \quad (31)$$

$$\text{prec.} = \frac{\text{TruePos.}}{\text{FalsePos.} + \text{TruePos.}} \quad (32)$$

$$F1 = 2 \times \left(\frac{\text{prec.} \times \text{rec.}}{\text{prec.} + \text{rec.}} \right) \quad (33)$$

where the Pos. and Neg. are abbreviations of positive and negative. Table 5 illustrates the above-mentioned metrics result. We have obtained high precision (0.86) using our proposed method.

In the last experiment that is reported in Table 6, we investigate the effect of different numbers of training samples on the accuracy. It is performed on CASME, CASME II, POVI, and FA which reaffirms the direct relationship between accuracy and numbers of training samples. However, our proposed method still keeps its performance even under severe reduction of training samples.

Finally, Fig. 8 compares the time consumption results with existing literature. According to the results, our

proposed method has less elapsed time than [4] and [21] planes in [4]. Moreover, in contrast to [21], it does not works. Since the proposed method, unlike [4], can require high learning time. automatically pick only one plane rather than many

Table 1: Apex spotting accuracy (%) on CASME with 15 training samples

Methods	Acc.
LBP on the 3 orthogonal planes [16]	31.2%
Cubic-LBP [2]	38.0%
LBP [17]	39.0%
LBP on the 4 planes [3]	45.1%
Combining PDE and Cubic-ULBP (ours)	81.2%

Table 2: Micro-changes spotting accuracy (%) on CASME II with 15 training samples

Methods	Acc.
LBP [17]	10.3%
Cubic-LBP [2]	20.1%
Combining PDE and Cubic-ULBP (ours)	61.0%

Table 3: Micro-changes spotting accuracy (%) using the proposed method (Combining PDE and Cubic-ULBP)

Dataset	Acc.
POVI	83.3%
FA	85.1%

Table 4: The obtained mean absolute error and standard error in our work

Dataset	mean absolute error	standard error
POVI	0.72	0.045
CASME	0.80	0.050
FA	0.63	0.040
CASME II	4.46	0.52

Table 5: Productivity of our proposed method (Combining PDE and Cubic-ULBP) using other metrics

Dataset	recall	<i>prec.</i>	F1
FA	0.82	0.86	0.84
CASME	0.79	0.82	0.81
POVI	0.84	0.81	0.82
CASME II	0.59	0.61	0.60

Table 6: Spotting accuracy (%) on CASME, CASME II, POVI, and FA with 5, 10, and 15 training samples

Method	Dataset	# training samples		
		5	10	15
Combining PDE and Cubic-ULBP (ours)	CASME	76.4	80.3	81.2
	CASME II	54.3	59.4	61.0
	POVI	77.8	82.1	83.3
	FA	79.1	83.9	85.1

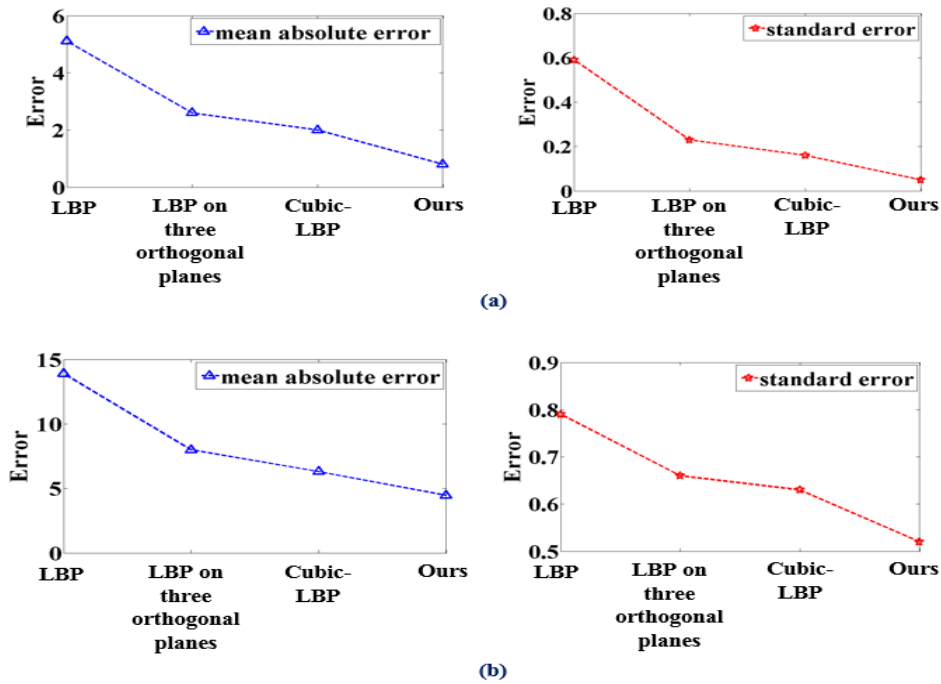


Fig. 7: Comparing error in other related methods and ours. (a) CASME (b) CASME II.

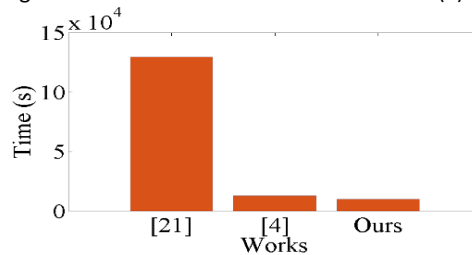


Fig. 8: Comparing the elapsed time of our proposed method with the existing works.

Conclusion

In our planet and even in cosmos, there are plenty of micro-changes. They contain significant information which should not be underestimated. Thus, spotting such tiny movements could be a bottleneck in wide range of applications from recognizing a liar to the health care system. Nevertheless, micro-change characteristics, namely low-intensity and brief appearance, make them almost invisible. In order to cope with this challenge, we proposed the novel approach which takes advantage of both Cubic-ULBP and PDE. Cubic-ULBP is robust against noise and illumination variation and at the same time could spot micro-changes in any direction. PDE is then applied to extract most effective features. According to our results, micro-change within the apex frame is located with a satisfying accuracy. In the future, the proposed PDE on the Cubic-ULBP could be used in similar scenarios, where the micro-changes need to be spotted. The limitation of the current work is the scarce number of 3D public datasets.

Author Contributions

Vida Esmaili: Conceptualization, Methodology, Investigation, Visualization, Analysis and interpretation, Data curation, Writing - original draft.

Mahmood Mohassel Feghhi: Methodology, Investigation, Writing - review & editing, Supervision, Data curation, Validation, Project administration, Formal analysis.

Seyed Omid Shahdi: Conceptualization, Investigation, Data curation, Visualization, Supervision, Validation, Analysis and interpretation, Writing - review & editing.

Conflict of Interest

The authors declare no potential conflict of interest regarding the publication of this work. In addition, the ethical issues including plagiarism, informed consent, misconduct, data fabrication and, or falsification, double publication and, or submission, and redundancy have been completely witnessed by the authors.

Abbreviations

<i>PDE</i>	Partial Differential Equations
<i>Cubic-ULBP</i>	Cubic Uniform Local Binary Pattern
<i>LBP-TOP</i>	Local Binary Pattern on Three Orthogonal Planes
<i>FA</i>	Fluorescein Angiography

References

- [1] P. Ekman, W. V. Friesen, "Nonverbal leakage and clues to deception," *Psychiatry*, 32(1): 88-106, 1969.
- [2] B. Yang, J. Cheng, Y. Yang, B. Zhang, J. Li, "MERTA: micro-expression recognition with ternary attentions," *Multimedia Tools Appl.*, 80(11): 1-16, 2021.
- [3] L. Zhou, X. Shao, Q. Mao, "A survey of micro-expression recognition," *Image Vision Comput.*, 105: 104043, 2021.
- [4] V. Esmaeili, S. O. Shahdi, "Automatic micro-expression apex spotting using Cubic-LBP," *Multimedia Tools Appl.*, 79(27): 20221-20239, 2020.
- [5] V. Esmaeili, M. M. Fegghi, S. O. Shahdi, "Micro-Expression recognition using histogram of image gradient orientation on diagonal planes," in *Proc. 2021 5th International Conference on Pattern Recognition and Image Analysis (IPRIA)*: 1-5, 2021.
- [6] V. Esmaeili, M. Mohassel Fegghi, S. O. Shahdi, "Autonomous apex detection and micro-expression recognition using proposed diagonal planes," *Int. J. Nonlinear Anal. Appl.*, 11: 483-497, 2020.
- [7] V. Esmaeili, M. Mohassel Fegghi, S. O. Shahdi, "A comprehensive survey on facial micro-expression: approaches and databases," *Multimedia Tools Appl.*, 81: 40089- 40134, 2022.
- [8] V. Esmaeili, M. Mohassel Fegghi, S. O. Shahdi, "Automatic micro-expression apex frame spotting using local binary pattern from six intersection planes," *arXiv preprint arXiv: 2104.02149*, 2021.
- [9] M. Xiao, Y. Chen, J. Zhu, H. Zhang, X. Zhao, L. Gao, W. Xing, "Climbing the apex of the ORR volcano plot via binuclear site construction: electronic and geometric engineering," *J. the Am. Chem. Soc.*, 141(44): 17763-17770, 2019.
- [10] K. S. Exner, "Does a thermoneutral electrocatalyst correspond to the apex of a volcano plot for a simple two-electron process?," *Angew. Chem. Int. Ed.*, 59(26): 10236-10240, 2020.
- [11] C. Widwijayanti, J. Déverchère, R. Louat, M. Sébrier, H. Harjono, M. Diament, D. Hidayat, "Aftershock sequence of the 1994, Mw 6.8, Liwa earthquake (Indonesia): Seismic rupture process in a volcanic arc," *Geophys. Res. Lett.*, 23(21): 3051-3054, 1996.
- [12] J. Skinner, "The smoke of an eruption and the dust of an earthquake: Dark tourism, the sublime, and the re-animation of the disaster location," in *the Palgrave handbook of dark tourism studies*. Palgrave Macmillan, London: 125-150, 2018.
- [13] O. Yildirim, M. Talo, E. J. Ciaccio, R. San Tan, U. R. Acharya, "Accurate deep neural network model to detect cardiac arrhythmia on more than 10,000 individual subject ECG records," *Comput. Methods Programs Biomed.*, 197: 105740, 2020.
- [14] E. Moghadas, J. Rezazadeh, R. Farahbakhsh, "An IoT patient monitoring based on fog computing and data mining: Cardiac arrhythmia usecase," *Internet Things*, 11: 100251, 2020.
- [15] S. T. Liong, J. See, K. Wong, R. C. W. Phan, "Less is more: Micro-expression recognition from video using apex frame," *Signal Process. Image Commun.*, 62: 82-92, 2018.
- [16] Y. Li, X. Huang, G. Zhao, "Can micro-expression be recognized based on single apex frame?," in *Proc. 2018 25th IEEE International Conference on Image Processing (ICIP)*: 3094-3098, 2018.
- [17] G. Zhao, M. Pietikainen, "Dynamic texture recognition using local binary patterns with an application to facial expressions," *IEEE Trans. Pattern Anal. Mach. Intell.*, 29(6): 915-928, 2007.
- [18] T. Ojala, M. Pietikäinen, D. Harwood, "A comparative study of texture measures with classification based on featured distributions," *Pattern Recogn.*, 29(1): 51-59, 1996.
- [19] T. Ojala, M. Pietikainen, T. Maenpaa, "Multiresolution gray-scale and rotation invariant texture classification with local binary patterns," *IEEE Trans. Pattern Anal. Mach. Intell.*, 24(7): 971-987, 2002.
- [20] V. Esmaeili, M. Mohassel Fegghi, S. O. Shahdi, "Micro-expression recognition based on the multi-color ulbp and histogram of gradient direction from six intersection planes," *J. Iran. Associ. Electr. Electron. Eng.*, 19(3): 123-130, 2022.
- [21] V. Esmaeili, M. Mohassel Fegghi, S. O. Shahdi, "Spotting micro-movements in image sequence by introducing intelligent cubic-LBP," *IET Image Process.*, 16(14): 3814-3830, 2022.
- [22] V. Esmaeili, M. Mohassel Fegghi, S. O. Shahdi, "Early COVID-19 diagnosis from lung ultrasound images combining RIULBP-TP and 3D-DenseNet," in *Proc. 2022 9th Iranian Joint Congress on Fuzzy and Intelligent Systems (CFIS)*: 1-5, 2022.
- [23] V. Esmaeili, M. Mohassel Fegghi, "Real-time authentication for electronic service applicants using a method based on two-stream 3d deep learning," *Soft Comput. J.*, 2023.
- [24] V. Esmaeili, M. Mohassel Fegghi, "Diagnosis of Covid-19 disease by combining hand-crafted and deep-learning methods on ultrasound data," *J. Mach. Vision Image Process.*, 9(4): 31-41, 2022.
- [25] V. Esmaeili, M. Mohassel Fegghi, "COVID-19 diagnosis: ULBPFP-net approach on lung ultrasound data," *Iran. J. Electr. Electron. Eng.*, 19(3): 2586-2586, 2023.
- [26] V. Esmaeili, M. Mohassel Fegghi, S. O. Shahdi, "Automatic micro-expression recognition using LBP-SIPI and FR-CNN," *AUT J. Model. Simul.*, 54(1): 59-72, 2022.
- [27] N. Wadhwa, M. Rubinstein, F. Durand, W. T. Freeman, "Phase-based video motion processing," *ACM Trans. Graphics (TOG)*, 32(4): 1-10, 2013.
- [28] H. Y. Wu, M. Rubinstein, E. Shih, J. Guttag, F. Durand, W. Freeman, "Eulerian video magnification for revealing subtle changes in the world," *ACM Trans. Graphics (TOG)*, 31(4): 1-8, 2012.
- [29] G. Fahmy, M. F. Fahmy, O. M. Fahmy, "Micro-movement magnification in video signals using complex wavelet analysis," *IET Image Process.*, 11(11): 986-993, 2017.
- [30] C. Liu, A. Torralba, W. T. Freeman, F. Durand, E. H. Adelson, "Motion magnification," *ACM Trans. Graphics (TOG)*, 24(3): 519-526, 2005.
- [31] M. Janatka, A. Sridhar, J. Kelly, D. Stoyanov, "Higher order of motion magnification for vessel localisation in surgical video," in *Proc. International Conference on Medical Image Computing and Computer-Assisted Intervention*: 307-314, 2018.
- [32] X. Li, X. Hong, A. Moilanen, X. Huang, T. Pfister, G. Zhao, M. Pietikäinen, "Towards reading hidden emotions: A comparative study of spontaneous micro-expression spotting and recognition methods," *IEEE Trans. Affective Comput.*, 9(4): 563-577, 2017.
- [33] M. Lu, Y. Chai, Q. Liu, "Observation of tower vibration based on subtle motion magnification," *IFAC-PapersOnLine*, 52(24): 346-350, 2019.
- [34] W. Fan, Z. Zheng, W. Zeng, Y. Chen, H. Q. Zeng, H. Shi, X. Luo, "Robotically surgical vessel localization using robust hybrid video motion magnification," *IEEE Rob. Autom. Lett.*, 6(2): 1567-1573, 2021.
- [35] A. Mohseni, "A new PDE-based resolution enhancement technique for the analysis of low SNR particle displacement images," *Eur. J. Mech. B.Fluids*, 85: 289-311, 2021.
- [36] T. Barbu, "Feature keypoint-based image compression technique using a well-posed nonlinear fourth-order PDE-based model," *Mathematics*, 8(6): 930, 2020.
- [37] L. Afraites, A. Hadri, A. Laghrib, M. Nachaoui, "A high order PDE-constrained optimization for the image denoising problem," *Inverse Probl. Sci. Eng.*, 29(12):1821-1863, , 2021.
- [38] A. K. Al-Jaberi, E. M. Hameed, "Topological data analysis for evaluating PDE-based denoising models," *J. Phys. Conf. Ser.*, 1897(1): 012006. 2021.
- [39] C. Fang, Z. Zhao, P. Zhou, Z. Lin, "Feature learning via partial differential equation with applications to face recognition," *Pattern Recogn.*, 69: 14-25, 2017.

- [40] S. Moorthi, S. Karthikeyan, "A Study On Learning Partial Differential Equations Algorithm For Face Recognition," *Int. J. Innovative Res. Explorer*, 5(4): 127-134, 2018.
- [41] W. J. Yan, Q. Wu, Y. J. Liu, S. J. Wang, X. Fu, "CASME database: A dataset of spontaneous micro-expressions collected from neutralized faces," in *Proc. 2013 10th IEEE International Conference and Workshops on Automatic Face and Gesture Recognition (FG)*: 1-7, 2013.
- [42] W. J. Yan, X. Li, S. J. Wang, G. Zhao, Y. J. Liu, Y. H. Chen, X. Fu, "CASME II: An improved spontaneous micro-expression database and the baseline evaluation," *PloS one*, 9(1): e86041, 2014.
- [43] A. J. Witsil, J. B. Johnson, "Volcano video data characterized and classified using computer vision and machine learning algorithms," *Geosci. Front.*, 11(5): 1789-1803, 2020.
- [44] W. Fuhl, T. Kübler, K. Sippel, W. Rosenstiel, E. Kasneci, "Excuse: Robust pupil detection in real-world scenarios," in *Proc. International Conference on Computer Analysis of Images and Patterns*: 39-51, 2015.
- [45] C. Nicholson, "Evaluation metrics for machine learning—accuracy, precision, recall, and F1 defined," ed: Pathmind.

Biographies



Vida Esmaili received her B.S. degree in Electrical Engineering from the Azad University of Abhar, Iran, in 2015 and the M.S. degree in Electrical Engineering from the Azad University of Qazvin, Iran, in 2018. Since 2019, she has been working toward the Ph.D. degree in Electrical Engineering at the Tabriz University, Iran. Her research interests include the area of image processing, machine learning, and pattern

recognition.

- Email: v.esmaeili@tabrizu.ac.ir
- ORCID: [0000-0002-1840-8659](https://orcid.org/0000-0002-1840-8659)
- Web of Science Researcher ID: AAB-9907-2022
- Scopus Author ID: 57215699025
- Homepage: <https://scholar.google.com/citations?user=lZvaGUYAAAAJ&hl=en>



Mahmood Mohassel Feghhi received the B.S. and M.S. degrees (with Honors) in Electrical Engineering from the Iran University of Science and Technology, Tehran, Iran, in 2006 and 2009, respectively, and the Ph.D. degree in Electrical Engineering from the College of Engineering, University of Tehran, Iran, in 2015. From 2007 to 2016, he held positions

as a senior design engineer in the areas of communication systems design with several Communications Industries and Inc. Since 2016, he has been with the Faculty of Electrical and Computer Engineering, University of Tabriz, Iran, where he is now an associate professor. His current research interests include network information theory, wireless networks, machine learning, resource allocation, scheduling and optimization.

- Email: mohasselfeghhi@tabrizu.ac.ir
- ORCID: [0000-0002-7193-843X](https://orcid.org/0000-0002-7193-843X)
- Web of Science Researcher ID: D-2414-2010
- Scopus Author ID: 27267677800
- Homepage: <https://asatid.tabrizu.ac.ir/en/pages/default.aspx?mohasselfeghhi>



Seyed Omid Shahdi received his B.S. degree in Electrical Engineering from the Azad University of Yazd, Iran, in 2006 and the M.S. degree in Electrical Engineering from the Azad University of Qazvin, Iran, in 2009 and the Ph.D. degree from the Universiti Teknologi Malaysia, Johor (Malaysia), in 2012. Currently, he is an assistant professor in the faculty of Electrical, Biomedical and Mechatronics Engineering, Qazvin Branch, Islamic Azad University, Qazvin, Iran. His

research interests include the areas of machine learning, pattern recognition, neural networks, and image processing. He has published many papers both at the national and international levels.

- Email: shahdi@qiau.ac.ir
- ORCID: [0000-0002-1827-1883](https://orcid.org/0000-0002-1827-1883)
- Web of Science Researcher ID: AAV-8113-2021
- Scopus Author ID: 36680945800
- Homepage: <https://old.qazvin.iau.ir/teacher/teacher.aspx?number=913780>

How to cite this paper:

V. Esmaili, M. Mohassel Feghhi, S. O. Shahdi, "Applying partial differential equations on cubic uniform local binary pattern to reveal micro-changes," *J. Electr. Comput. Eng. Innovations*, 12(1): 259-270, 2024.

DOI: [10.22061/jecei.2023.9600.639](https://doi.org/10.22061/jecei.2023.9600.639)

URL: https://jecei.sru.ac.ir/article_2012.html

